We are IntechOpen, the world's leading publisher of Open Access books Built by scientists, for scientists

4,800
Open access books available

122,000
International authors and editors

135M
Downloads

Our authors are among the

154
Countries delivered to

TOP 1%
most cited scientists

12.2%
Contributors from top 500 universities

CLARIVATE ANALYTICS BOOK CITATION INDEX INDEXED

WEB OF SCIENCE™

Selection of our books indexed in the Book Citation Index in Web of Science™ Core Collection (BKCI)

Interested in publishing with us?
Contact book.department@intechopen.com

Numbers displayed above are based on latest data collected.
For more information visit www.intechopen.com

6

Effect of Hydrothermal Self-Healing and Intermediate Strengthening Layers on Adhesion Reinforcement of Plasma-Sprayed Hydroxyapatite Coatings

Chung-Wei Yang and Truan-Sheng Lui
Department of Materials Science and Engineering, National Formosa University,Yunlin,
Department of Materials Science and Engineering,
National Cheng Kung University, Tainan,
Taiwan

1. Introduction

Biomaterials employed in calcified hard tissue repair generally serve the purpose of load carrying in cases of fractures, defects and joint replacement. Metallic materials are more suitable for load-bearing applications compared with ceramics and polymeric materials due to their combination of high mechanical strength and fracture toughness. Among generally used metallic biomaterials such as 316L stainless steel and Co-Cr-Mo alloys (ASTM F75), grade II commercial pure titanium (ASTM F67) and Ti-6Al-4V alloys (ASTM F136ELI) exhibit the most suitable characteristics for biomedical applications because of their high biocompatibility, specific strength and corrosion resistance [Niinomi, 2001]. The apparent success of titanium and its alloys in implants has been attributed to the existence of a thin, stable passivation TiO_2 layer. Another advantage of titanium and its alloys for using in hard tissue replacements is their low Young's modulus because a low Young's modulus equivalent to that of human cortical bone is simultaneously required to inhibit stress shielding effect and bone absorption [Pilliar et al., 1979; Kuroda et al., 1998; Niinomi et al., 2002]. Nowadays, they are commonly clinical used in hard tissue implants such as artificial hip prosthesis, knee joints and dental roots. A biological fixation between these hard tissue implants and surrounding bones can be successfully achieved by the bone ingrowth with a mechanical interlocking [Engh et al., 1987; Callaghan, 1993]. However, limitations of metallic biomaterials are the release of toxic metallic ions and corrosion/wear products into surrounding tissues and fluids [Sunderman et al., 1989; Healy & Ducheyne, 1992; Niinomi et al., 1999; Akahori et al., 2004].

In the biomedical applications, another concept to design a bioactive surface fixation has been achieved by the bone apposition method. Bioactive ceramics have often been used as coatings to modify the surface and create a new surface for the bioinert metallic implants. With the same chemical and crystallographic structure as the major inorganic constitute of hard tissues, bioactive hydroxyapatite ($Ca_{10}(PO_4)_6(OH)_2$, HA) is a widely preferred calcium phosphate bioceramic, which is considered as suitable bone graft substitutes [Holmes et al.,

1986; Bucholz et al., 1989] in both dentistry and orthopaedics due to its favorable bioactive properties and osteoconductivity [Munting et al., 1990; Jansen et al., 1991; Yuan et al., 2001]. The advantages of HA including: (1) earlier stabilization, rapid fixation and stronger chemical bonding between the host bone and the implant [Jansen et al., 1991; Hench, 1991; Schreurs et al., 1996], and (2) increased uniform bone ingrowth and ongrow the bone-implant interface. In spite of the good biocompatibility and osteoconductivity of HA, the limitations for the usage of the dense HA sintering bulks for bone replacement are their low fracture toughness [van Audekercke & Martens, 1984] and bending strength under load-bearing situations [de Groot et al., 1990; Choi et al., 1998]. Therefore, HA is generally applied as coatings for the purpose of improving the bioactivity of the bioinert metallic implants including the stem and the acetabular cup. The combination of high strength metallic substrates with osteoconductive properties of bioceramic makes HA-coated titanium implants attractive for the load-bearing situations in orthopedic and dental surgery. In addition to promote earlier stabilization of the implant with surrounding bone, another reason for coating HA is to extend the functional life of the prosthesis and to improve the adhesion of the prosthesis to the bone. Studies demonstrated that HA-coated titanium implants show higher push-out strength compared to uncoated titanium implants [Geesink et al., 1988; Wolke et al., 1991; Cook et al., 1992; Wang et al., 1993a], and post-mortem studies reported direct bone contact with implants without a fibrous tissue interface in patients who have had successful HA-coated total hip arthroplasties [Bauer et al., 1991; Lintner et al., 1994]. Moreover, the bone bonding capacity of the HA coatings can help cementless fixation of orthopedic prostheses. It has been shown that the skeletal bonding is enhanced immediately after implantation [Jarcho, 1981; Geesink et al., 1987; Cook et al., 1988].

Advances in coating technology have brought about a new dimension in processing of biomaterials. It is clear that surface modification of metallic biomaterials gives rise to enhance biocompatibility. Many coating techniques have been used for HA coatings preparation onto metallic substrates, including plasma spraying [Wang et al., 1993b; Gross & Berndt, 1998], HVOF spraying [Sturgeon & Harvey, 1995; Lugscheider et al., 1996], chemical vapor deposition (CVD) [Liu et al., 2007], physical vapor deposition (PVD, including the RF-sputtering method) [Ozeki et al., 2006], sol-gel coating [Ben-Nissan & Choi, 2006], electrochemical deposition [Peng et al., 2006], electrophoresis method [Wei et al., 2005], and biomimetic coating methods [Kokubo et al., 1987]. The HA coatings obtained from these various techniques differ in chemistry and crystallinity, which will affect the biological responses and their performances. Therefore, in addition to consider biological advantages of fast bony adaptation, firm implant-bone attachment, reduced healing time of HA to surrounding bone, the phase composition, mechanical properties and operation feasibility of HA-coated implants should also be considered for using in long-term load-bearing applications of dental implants and orthopedic prostheses. Compared with these techniques, plasma spraying constitutes the state-of-the-art procedure to improve the biological integration implants and the main industrial process to deposit thick HA coatings. The attraction lies in its easy operation, relatively low substrate temperature, high HA coating efficiency and its ability to deposit tailored HA coatings on implants with complex shapes.

The plasma spraying process was patented in 1960s, and the technical utilization of plasma as a high-temperature source is realized in the plasma torch. The torch operates with a central cone-shaped tungsten cathode and a water-cooled cylindrical copper anode. A typical plasma spraying process is shown in Fig. 1 [Suryanarayanan, 1993]. The principle of

plasma spraying is that inducing an arc by a high current density and a high electric potential between the anodic copper nozzle and tungsten cathode. The plasma gases flow is injected into the annular gap between the two electrodes, and an arc is initiated by a high-frequency discharge. Noble gases of helium (He) and argon (Ar) are usually used as the primary plasma-generating gas. Diatomic gases of hydrogen (H_2) and nitrogen (N_2) can be used as the secondary gas to increase the enthalpy of plasma torch. As the plasma gases pass around the arc created between the electrodes, they are heated and partially ionized emerging from the nozzle with high velocity and high temperature. For atmospheric plasma spraying (APS), the processing temperatures are typically in the range of 1×10^4 to 1.5×10^4 K depending on the type of the plasma gas used and the power input. Factors influence the degree of particles melting during plasma spraying includes variables which control the temperature of the plasma, such as current density, anode-cathode gap distance and gas mixture. The widely used plasma-generating gas is pure Ar (purity > 99.95 wt. %).

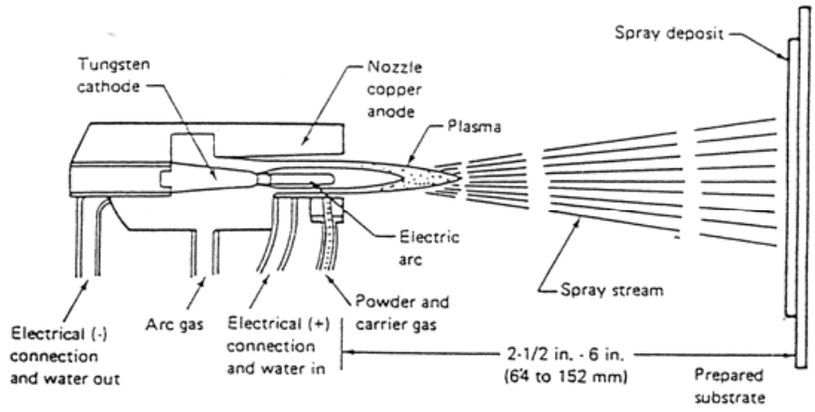

Fig. 1. Schematic illustration of plasma spraying process operation.

Since the thermal conductivity and the heat conduction potential for diatomic gases, such as H_2 and N_2, are much higher than Ar [Bourdin et al., 1983], a mixed gas composition with Ar and H_2/N_2 gives a quite hotter plasma torch than 100% Ar gas. Figure 2 displays the variation of heat content and temperature during ionization and dissociation stages of these plasma gases [Ingham & Shepard, 1965]. When well-crystallized HA powders are injected into the high temperature plasma torch, small granules will be evaporated in the torch, and larger particles are melted or partial-melted quickly by the high temperature plasma torch. Then these melted droplets are accelerated to about 200 m/s before impacting the substrate [Fauchias et al., 1992; Pfender, 1994]. The high impact velocity supplies high kinetic energy, which is expended in spreading the molten or semi-molten droplets and creating a lamellar microstructure. In addition, high cooling rate upon impact is estimated to be of the order of 10^6 to 10^8 K s^{-1}. Therefore, the large contact area with the substrate and the rapid solidification result in producing amorphous calcium phosphate (ACP) component within coatings, and it is more commonly found at the coating/substrate interface.

Because of the extremely high temperature, high enthalpy of the plasma torch and rapid solidification, a significant phase transformation or decomposition of HA is occurred during the plasma spray coating process. It results in large scale dehydroxylation and decomposition effects of crystalline HA phase into tri-calcium phosphate ($Ca_3(PO_4)_2$, TCP),

tetra-calcium phosphate ($Ca_4P_2O_9$, TP), calcium oxide (CaO), oxyhydroxyapatite and ACP within the sprayed coatings. Plasma-sprayed HA coatings (HACs) with a higher content of impurity phases and ACP component will display higher dissolution rate than crystalline HA in aqueous solutions and body fluids [Ducheyne et al., 1993; Radin & Ducheyne, 1993]. It results in some problems with decreasing the structural homogeneity and the degradation of mechanical properties in the firm fixation between the implant and surrounding bone tissue [C.Y. Yang et al., 1995, 1997]. Therefore, decreasing the impurity phases and ACP is important for the long-term mechanical and biological stability of plasma-sprayed HACs. The ACP is a thermodynamically meta-stable component and impurity calcium phosphate phases are undesirable for the HACs, studies pointed out that performing appropriate thermal treatments, such as air or vacuum heat treatments, spark plasma sintering (SPS) technique, and hydrothermal treatments, etc., are available methods to significantly promote HA crystallization and to improve the mechanical properties and biological responsibility of HACs [Ji & Marquis, 1993; Wang et al., 1995; Lee et al., 2005; Yu et al., 2003; C.W. Yang & Lui, 2008].

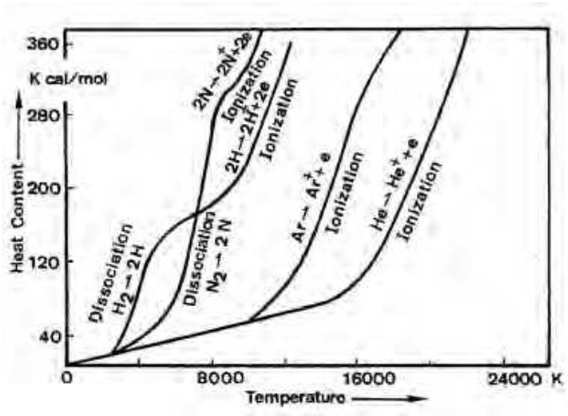

Fig. 2. The variation of heat content and temperature during ionization and dissociation stages of various plasma gases.

Although a thick, tailored HA coating can easily be applied by the plasma spraying process, a limitation of the HACs for applications is its low cohesion and adhesive bonding strength. To solve these problems, it has been generally recognized that performing post-heat treatments is an effective way to improve the bonding strength of HACs. Pure HACs is brittle, thus, some bioinert ceramics or metals, such as dicalcium silicate (β-Ca_2SiO_4) aluminum (Al_2O_3), partially stabilized zirconia (PSZ), titania (TiO_2), titanium and its alloys, have been chosen as the reinforcing additives to fabricate HA/ceramics pre-composite powders [Choi et al., 1998; Zheng et al., 2000; Chou & Chang, 2002a; Y. Yang & Ong, 2003; Sato et al., 2008; Cannillo et al., 2008]. The plasma-sprayed composite coatings made from HA and these reinforcing additives can help to alleviate the brittleness of pure HA and to improve the mechanical properties of HACs, as well as the reinforcements. Since a continuous ACP layer is resulted from rapid solidification of crystalline HA droplets, it is thought of acting a high solubility region and a low energy fracture path. This situation will result in weakening the mechanical integrity of the HA coating/substrate interface and further decreasing the adhesive bonding strength. Therefore, another way to improve the interfacial strength is the application of a stable bioinert intermediate strengthening layer, or

so-call as bond coat, at the coating/substrate interface to enhance the adhesion of HACs to metallic substrates. The bond coat can reduce the thermal gradient at the interface to decrease significant thermal decomposition of HA. The bond coat can help to prevent the release of metal ions to the surrounding tissue. It can also provide better mechanical interlocking and even establish a chemical bonding between bond coat and HACs. Many attempts have been made to apply the above-mentioned bioinert ceramics or metals as bond coat materials to improve the performance of plasma-sprayed HACs [Lamy et al., 1996; Chang et al., 1997; Kurzweg et al., 1998; Fu et al., 2001; Lu et al., 2004].

Plasma-sprayed HACs with a better bonding strength can be achieved by adding reinforced additives to form composite coatings and applying heat treatments to acquire a higher HA crystallinity level and fewer coating defects as a result of HA crystallization. With different materials preparation, manufacturing and characterization, or different *in vitro* and *in vivo* examination methods, however, it is difficult to systematically evaluate the relationship between the HA crystallization, interfacial chemical reactions, biological responses and mechanical properties of the coatings. This chapter represents the crystallization effect on influencing the bonding strength of the plasma-sprayed HACs through performing post-vacuum heating and hydrothermal treatments. The benefit of low-temperature hydrothermal crystallization on plasma-sprayed HACs is clarified through the evaluation of crystallization mechanism by the Arrhenius kinetics. Through adding a ceramic and a metallic bond coat, the effects of mechanical interlocking and interfacial chemical reactions at interface on improving the bonding strength of HA/bond coat will be discussed. Since variables associated with implants preparation result in a certain extent of fluctuation for material properties, a strong reliability of implants is required when they are extrapolated to clinical applications. To determine the failure probability and reliability, the failure surface morphologies of HACs and the Weibull model of survival analysis [Weibull, 1951] were used to assess the effects on bonding strength data fluctuation pertaining to microstructural feature and the reliability of HACs.

2. Processing

Medical grade high purity HA (Sulzer Metco XPT-D-701) powder with particle size ranging from 15 to 40 μm were used in the coating process. Commercial yttria-stabilized zirconia (ZrO_2, YSZ, Amdry 142F), pure α-titanium (CP-Ti, Amdry 9182) powders were selected as bond coat materials, and Ti-6Al-4V alloys (ASTM F136 ELI) were selected as substrates. Prior to spraying, substrates were grit-blasted with SiC grit to roughen the surface. The average surface roughness (Ra) of grit-blasted substrate was controlled at about 3.9±0.3 μm. The powders were carried by high purity Ar gas to the plasma torch following the spraying parameters as listed in Table 1. The coating thickness of YSZ and CP-Ti bond coats was controlled at about 30 μm. Total coating thickness of 120±10 μm was prepared for HA coatings with and without intermediate layers. Table 2 lists the surface roughness of YSZ, CP-Ti bond coats and HA top coat of composite coatings.

Post-heat treatments were performed in a vacuum heating chamber (Vacuum industries, System VII) with 1.33×10^{-3} Pa at 600°C (named as V-HACs) with a heating rate of 10°C/min, held for 3h and then furnace cooling. The hydrothermal treatment was carried out in a hermetical autoclave (Parr 4621, Pressure Vessel) at 150°C for 6h (named as HT-HACs). The heating temperature was maintained throughout the experiments using a

heater attached to the autoclave and the temperature was precisely controlled by a Parr 4842, PID controller with ± 1°C. The autoclave contained 100 ml deionized water, which was used as the source of steam atmosphere during the hydrothermal treatment, and the saturated steam pressure at 150°C was 0.48 MPa. The specimens were isolated without the immersion in the water. Phase compositions of the YSZ, CP-Ti bond coats and plasma-sprayed HACs were identified by X-ray diffraction (Rigaku D/MAX III. V), using CuKα, operated at 30 kV, 20 mA. A commonly used index of crystallinity (IOC) was adopted for the purpose of further quantitatively evaluating the crystallization state of the vacuum and hydrothermally-treated HACs. The IOC data is a ratio of three strongest HA diffraction peaks ((211), (112), (300), JCPDS 9-432) integral intensity of the HACs (*Ic*) and the as-received HA powder (HAP, *Ip*) according to the relationship IOC = (*Ic*/*Ip*) × 100%. This method supposes that the IOC of as-received HAP is 100% and the calculated IOC value of the as-sprayed HACs is about 20%. To realize the variation of TCP, TP and CaO impurity phases after applying heat treatments, the internal standard method was used to quantitatively determine these phase content within the heat-treated HACs. The integral intensity of known weight percent pure Si powder added in the specimens was taken as internal standard. The calibration curves for impurity phase content have been established by Wang et al. [Wang et al., 1995]. The main peak integral intensity ratio between TCP, TP and CaO phases from various XRD patterns of V-HACs and HT-HACs were compared to the calibration curves and the concentrations (in wt. %) in these specimens were calculated.

Spraying parameters	YSZ bond coat	CP-Ti bond coat	HA top coat
Coating thickness (μm)	30	30	120/90 †
Primary gas (*l*/min)	Ar (41)	Ar (46)	Ar (41)
Secondary gas (*l*/min)	H_2 (10)	H_2 (6)	H_2 (8)
Power (kW)	42.5	38.4	40.2
Powder carrier gas (*l*/min)	Ar (3)	Ar (3)	Ar (3)
Powder feed rate (g/min)	20	20	20
Surface speed (cm/min)	8000	8000	8000

† 90 μm was prepared for the HA top coat of HA/YSZ, HA/CP-Ti composite coatings, and 120 μm was prepared for plasma-sprayed HA coatings without bond coats.

Table 1. Plasma spraying parameters employed for preparing HA composite coatings.

Grit-blasted Ti-6Al-4V	YSZ bond coat	CP-Ti bond coat	Plasma-sprayed HACs	HAC/YSZ coating	HAC/CP-Ti coating
3.9 ± 0.3	6.4 ± 0.4	6.4 ± 0.2	7.6 ± 0.7	8.7 ± 1.1	8.9 ± 0.7

Note: values are given as mean ± S.D., each value was the average of ten tests (*n*=10).

Table 2. Surface roughness (Ra, μm) of the substrate and various plasma-sprayed coatings.

3. Microstructural evolution and biological responses of heat-treated HA coatings

Figure 3(a) shows the phase composition of as-sprayed CP-Ti bond coat. In addition to the diffraction peaks of titanium (α-Ti), the oxidation product of α-Ti within the coating is $TiO_{1.04}$, which represents two different crystal structures: the major oxide is cubic $TiO_{1.04}$ (JCPDS 43-1296) and the main peak another oxide of hexagonal $TiO_{1.04}$ is observed at 2θ = 36° (JCPDS 43-1295). The as-sprayed YSZ bond coat remains a cubic crystal structure (JCPDS 27-0997) as shown in Fig. 3(b). Figure 3(c) shows the phase composition of as-sprayed HACs. A fairly high content (about 49.3 wt. %) of ACP and impurity calcium phosphate phases, including α-$Ca_3(PO_4)_2$ (α-TCP), β-$Ca_3(PO_4)_2$ (β-TCP), $Ca_4P_2O_9$ (TP) and CaO, are identified in the as-sprayed HACs besides the desired HA phase.

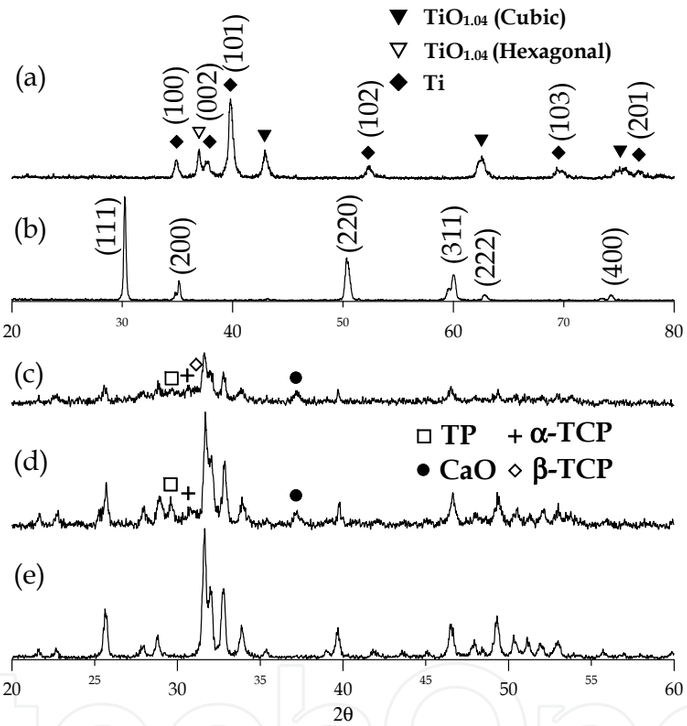

Fig. 3. X-ray diffraction patterns of plasma-sprayed (a) CP-Ti bond coat, (b) YSZ bond coat, (c) as-sprayed HACs, (d) V-HACs and (e) HT-HACs coatings.

Figure 3(d) displays the X-ray diffraction patterns of post-vacuum heat treated coatings (V-HACs). The TCP, TP and CaO impurity phases still remained within coatings after performing 600°C vacuum heat treatment, at which the total impurity phase content within V-HACs is about 20.3 wt. %. The quantitative result of the IOC for V-HACs is about 70%. According to the phase diagram of CaO-P_2O_5 system, since there is a lack of ambient partial water vapor pressure during vacuum heating, TCP and TP phases are stable phases and they cannot be eliminated without the replenishment of hydroxyl groups (OH^-). The CaO remained within the V-HACs because it cannot easily be converted into HA if the ambient heating atmosphere without abundant H_2O molecules [Weng et al., 1996; Cao et al., 1996]. It is worth noting that these TCP, TP and CaO impurity phases are significantly eliminated

after hydrothermal treatment as shown in Fig. 3(e). The impurity phase content within HT-HACs is about 12.1 wt. %. The sharpening of three strongest HA main peaks and the flattening of the diffraction background (2θ at about 28° to 34°) mean that the plasma-sprayed HACs further crystallized and the content of ACP significantly decreased by the 150°C hydrothermal treatment in an ambient saturated steam pressure system. The IOC of HT-HACs is about 66%, which is close to the high-temperature vacuum heat treatment. Since the hydroxyl groups promote the reconstitution of ACP into crystalline hydroxyapatite [Tong et al., 1997], therefore, the saturated steam pressure atmosphere of autoclaving hydrothermal treatment can effectively improve HA crystallization and effectively eliminate the ACP and impurity phases of plasma-sprayed HACs with the replenishment of hydroxyl groups.

Figure 4(a) shows the typical surface morphology of the plasma-sprayed HACs, which represents an accumulated molten splats feature with a fair amount of pores and thermal-induced microcracks at the rapid cooling stage. After applying 600°C vacuum het treatment, Fig. 4(b) also shows a surface cracking feature for the V-HACs specimens. Different from the thermal contraction cracking during plasma spraying, however, these cracks are resulted from the significant crystallization-induced contraction effect [C.W. Yang et al., 2006] during high-temperature crystallization of HACs. Figure 4(c) displays the typical coating surface of HT-HACs, which provides evidence in microscopic surface features different from that of as-sprayed HACs and V-HACs. It is worth noting that nano-scale crystalline growth, indicated by the circle in Fig. 4(c), is observed on the surface of the HT-HACs specimen. These particles can be attributed to HA crystallites, which crystallized from the hydroxyl-deficient structure of plasma-sprayed HACs through the replenishment of hydroxyl groups. In addition, since the ACP is more soluble than crystalline HA phase in an aqueous environment, part of the new-growth crystalline HA might have formed through a dissolution-recrystallization process. The nano-scale HA crystalline experiences further grain growth with a larger crystal size in the vicinity of microcracks as indicated by the arrow. The reduction of coating defects for hydrothermally-treated HACs can be recognized as the self-healing effect of the hydrothermal treatment [C.W. Yang & Lui, 2008]. As a result of crystallization during heat treatments, the contraction-induced cracking and the self-healing phenomena will significantly influence the bonding strength and the failure mechanism of HACs.

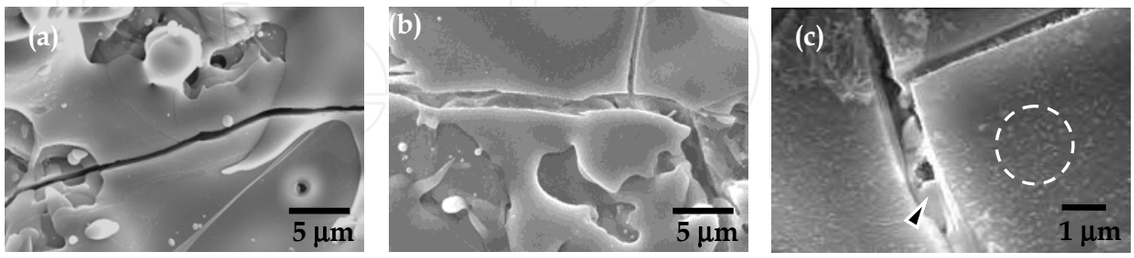

Fig. 4. Surface morphologies of (a) as-sprayed HACs, (b) V-HACs and HT-HACs coatings.

Figure 5 shows the cross-sectional microstructures of the as-sprayed HACs, V-HACs, HT-HACs and various composite coatings. According to the quantitative calculation by an image analyzer, the spraying defects content (in volume %), including pores and thermal-induced microcracks, is about 3.9 % for as-sprayed HACs in the case of Fig. 5(a). Since a significant volume contraction during HA crystallization [C.W. Yang & Lui, 2007], the V-

HACs specimen shows a coating structure with many vertical, apparent contraction-induced cracks as indicated by the arrow in Fig. 5(b). The defects content of V-HACs coating is about 5.3%. As shown in Fig. 5(c), the HT-HACs possess significant fewer microcracks and lower defects content (about 2.6%). It displays a much denser microstructure than the as-sprayed HACs and V-HACs. The self-healing effect of hydrothermal crystallization resulted from the new-growth HA crystallites can be recognized to diminish the coating defects and further increase the densification of plasma-sprayed HACs. Figure 5(d) and 5(e) shows the cross-sectional features of HA/CP-Ti and HA/YSZ composite coatings, respectively. The HA top coat shows a similar microstructure to the as-sprayed HACs. Since the bond coat can reduce the thermal gradient at HA/substrate interface, the HA top coat in Fig. 5(d) and 5(e) shows less thermal-induced microcracks for these composite coatings. The coating thickness of both CP-Ti and YSZ bond coats is about 30 μm, and the Ti-6Al-4V substrate is fully covered by the bond coat. In addition, the CP-Ti and YSZ bond coats provide a rougher surface than the substrate (refer to Table 2) to the HAC top coat. This can help to improve the mechanical interlocking between HA/substrate interface and further increase the adhesive bonding strength of the HA coatings.

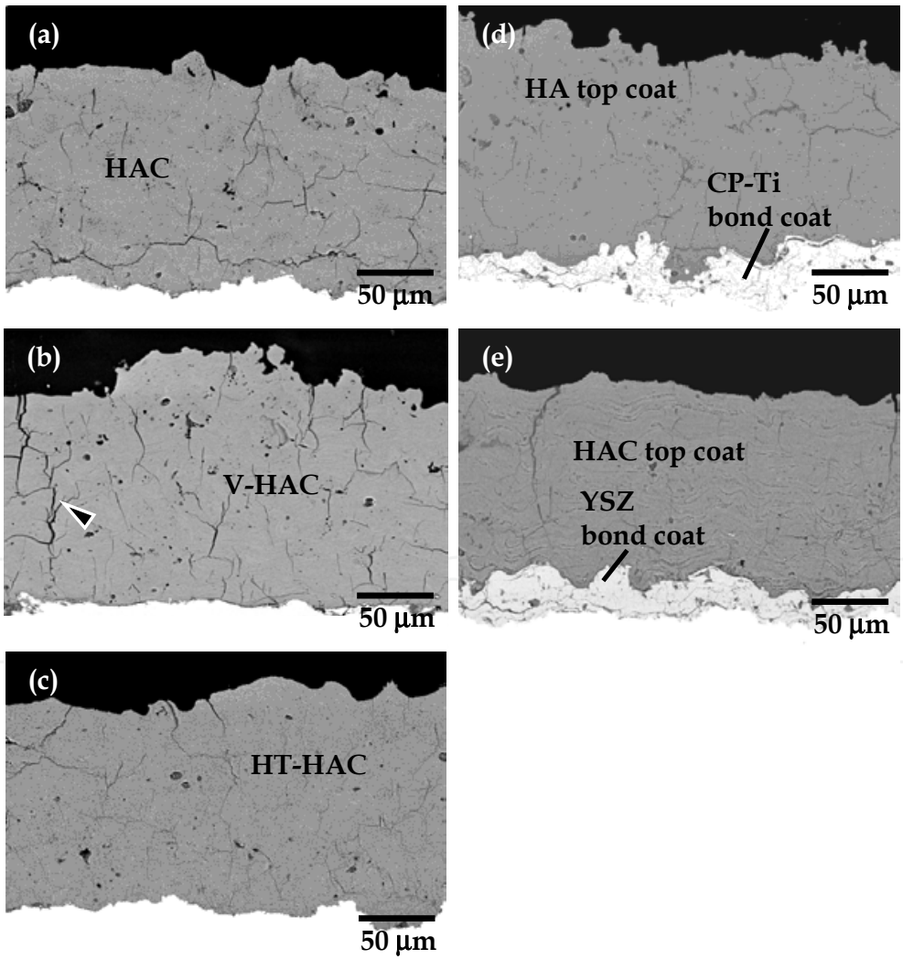

Fig. 5. Cross-sectional images of (a) as-sprayed HACs without bond coat, (b) V-HACs coating, (c) HT-HACs coating, (d) HA/CP-Ti and (e) HA/YSZ composite coatings.

In addition, the biological responses of plasma-sprayed HACs, V-HACs and HT-HACs are quantitatively evaluated *in vivo* using the Chinese coin implant model in the femoral of a goat, and details of the experimental procedure have been well described in the previous reports [C.Y. Yang et al., 2007, 2009]. The osteoconductivity of the implants is evaluated quantitatively in terms of the new bone healing index (NBHI), which defined as the (area of new bone/area of surgical defect region) × 100%. The ability of osseointegration of implants is addressed as apposition index (AI), which defined as the (length of direct bone-implant contact/total length of bone-implant interface) × 100%. This method can help to determine the success or failure of an implant by evaluating the interaction occurring at the bone-biomaterial interface. The mean NBHI and AI data listed in Table 3 indicated that the crystallized HACs with applying heat treatments have a statistically higher extent of new bone healing and apposition index compared to the as-sprayed HACs after 12 weeks of implantation. Figure 6 shows the amount of new bone increased within the surgical defective bone regions of as-sprayed HACs, V-HACs and HT-HACs after 12 weeks of implantation. Since the phase composition and crystallinity of post-heat-treated HACs remain stable at 12 weeks, it provides better treated-HACs-to-bone contact area, which can provide the firm bone/implant fixation compared to as-sprayed HACs. Considering the crystallized coatings of V-HACs and HT-HACs, hydrothermally-crystallized HACs show better *in vivo* biological responses at 12 weeks and show the potentiality to provide biological fixation than the other condition in the present results.

	Plasma-sprayed HACs †	V-HACs †	HT-HACs †
NBHI ‡ (%)	74.7 ± 6.6	77.8 ± 5.1	79.0 ± 7.5
AI ‡ (%)	67.3 ± 7.1	76.8 ± 5.7	78.1 ± 6.4

† Values are given as an average ± standard deviation (SD).
‡ NBHI: new bone healing index. AI: apposition index.

Table 3. NBHI and AI values for plasma-sprayed HACs, V-HACs and HT-HACs after 12 weeks of implantation.

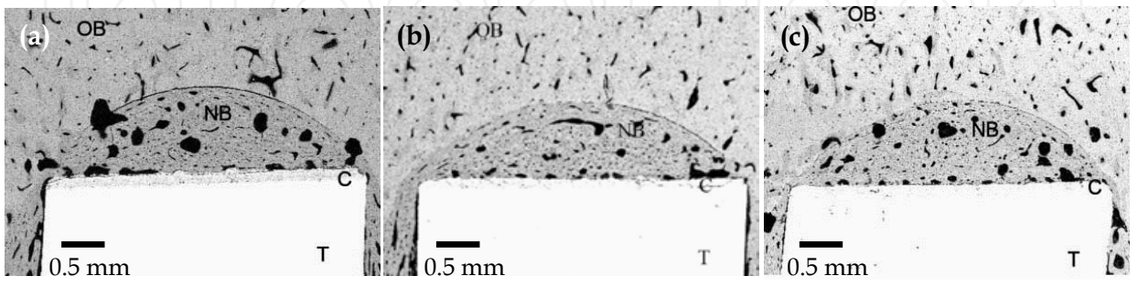

Fig. 6. SEM/BEI of histological section at the surgical defect region for 12 weeks post-implantation: (a) plasma-sprayed HACs, (b) V-HACs and (c) HT-HACs. The new bone is repaired within the surgical defect regions of these coatings. The osseointegration is found at the bone/HA coating interfaces (T: Ti-6Al-4V, C: coating, NB: new bone, OB: old bone).

4. Affected factors on crystallization during heat treatments

The experimental results demonstrate that the autoclaving hydrothermal treatment can actually promote significant crystallization to improve the phase purity, crystallinity, microstructural homogeneity and biological responses of plasma-sprayed HACs. Previous studies have indicated that the kinetics of crystallization and chemical reactions during heat treatments are significantly related to heating temperatures, which is recognized as a main factor for promoting HA crystallization [Chang et al., 1999; Campos et al., 2002; Roeder et al., 2006]. Since the IOC value represents the degree of crystallization for heat-treated HACs, it can be recognized of the conversion ratio from ACP to crystalline HA under different heating conditions. Considering the theory of chemical reaction kinetics and the definition of IOC for crystallized HACs, the HA crystallization process should follow the Arrhenius equation [Chang et al., 1999; Huang et al., 2000; Liu et al., 2001; C.W. Yang & Lui, 2007] as represented in Eq. (1). Based on the reaction kinetics of Arrhenius equation, the rate constant (k) can be thought as the reaction rate, and it represents the crystallization rate during heat treatments. The reaction rate and the activation energy of HA crystallization within vacuum can be quantitatively evaluated by the IOC of each specimens and HA crystallization under the vacuum heating follows the second-order Arrhenius reaction kinetics.

$$r = \frac{dIOC}{dt} = k(1 - IOC)^2 \tag{1}$$

However, a significant crystallization of hydroxyl-deficient HACs requires at least 600°C [Gross et al., 1998; Feng et al., 2000; Lu et al., 2003], and high heating temperatures tend to undermine the structural integrity and cause phase decomposition of crystalline HA. In addition, the effect of the ambient heating atmosphere is another factor that should be considered to affect the reaction rate for HA crystallization. Referring to the phase diagram of $CaO\text{-}P_2O_5$ at 500 mmHg partial steam pressure (P_{vapor}), HA is a stable phase and water vapor is a significant factor to promote HA crystallization. The low-temperature hydrothermal treatment system with a surrounding saturated steam pressure can help to diminish the ACP, impurity phases within the plasma-sprayed HACs and significantly promote HA crystallization. This is a result of replenishment of missing OH^- groups with surrounding H_2O molecules [Chen et al., 1997; Y. Yang et al., 2003]. Thus, the influence of ambient water vapor during the autoclaving hydrothermal treatment should be considered to evaluate the kinetics of the hydrothermal crystallization at lower heating temperatures.

Since the dehydroxylation is a result of hydroxyl groups (OH^-) broken away from HA crystal structure during plasma spraying process, the ACP with a reduced crystallinity of HA occurred in the coating layers. When the hydrothermal treatment is applied to promote the crystallization of plasma-sprayed HACs, the water is vaporized. The ionized water vapor molecules contain H^+ and OH^- groups within the hermetical autoclave and the content of H^+ and OH^- groups increases with increasing the temperature [Zhang et al., 2001]. The resultant OH^- groups within the water vapor atmosphere are expected to react with ACP and other low-crystalline calcium phosphate components, and convert them into crystalline HA phase through the replenishment of OH^- groups. The previous study has demonstrated that the reaction order under the hydrothermal crystallization not only depends on the effects of heat treatment time and temperatures, but the saturated steam pressure (P_{vapor}) factor is involved at each hydrothermal heating temperature [C.W. Yang &

Lui, 2009]. According to a series of examinations, Eq. (2) concludes the modified form which involves a saturated steam pressure term following the second-order reaction kinetics of Arrhenius equation.

$$r = \frac{dIOC}{dt} = k(1 - IOC)^{3/2} P_{vapor}^{1/2} \tag{2}$$

Experimental evidence confirmed that the ambient saturated steam pressure plays an important role in lowering heating and reactions temperatures. This results in a significant microstructural self-healing effect through the grain growth of HA nanocrystallite [C.W. Yang & Lui, 2009], as shown in Figs. 4(c), within the hydrothermally-crystallized HACs, which also shows a statistically higher extent of new bone apposition [C.Y. Yang et al., 2007] essential in the initial fixation of implants in clinical applications.

The XPS analysis results clarify the replenishment of OH^- groups and the reduction of the dehydroxylation state of hydroxyl-deficient HACs during the hydrothermal treatment. Figure 7 shows the high resolution XPS O 1*s* spectra of HA coatings with curve-fittings, which resulted from the Gaussian peak-fitting routine. The corresponding O 1*s* band of the as-sprayed HACs presented in Fig. 7(a) consists of three components at about BE = 531.4 eV, BE = 532.4 eV and BE = 533.2 eV, which correspond to the PO (PO_4^{3-}), POH bonds of HA crystal and the surface adsorbed H_2O. The adsorbed H_2O peak represents that the surface of the as-sprayed HACs is easily affected by the surrounding moisture within the air, and H_2O molecules can be physically adsorbed on the HACs.

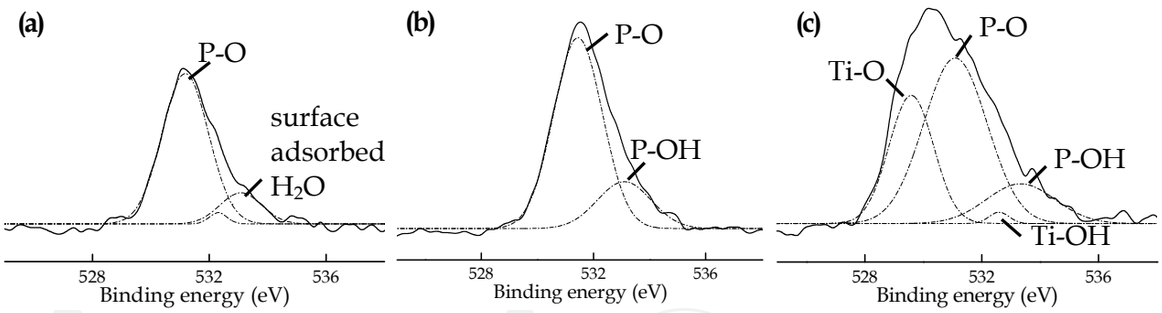

Fig. 7. XPS O 1*s* spectra curve-fitting results of (a) plasma-sprayed HACs, (b) HT-HACs, and (c) the surface close to the HT-HACs/Ti-substrate interface.

In contrast with the as-sprayed HACs, XPS O 1*s* spectra of hydrothermally-treated coatings (HT-HACs) with relatively large integration area of the POH bonding peak but without the adsorbed H_2O peak is shown in Fig. 7(b). The surface residual adsorbed H_2O molecules can be seen to be reduced. The hydroxyl-deficient state of the as-sprayed HACs is significantly improved with the abundant replenished OH^- groups from the hydrothermal treatment, especially under a higher saturated steam pressure atmosphere. In Fig. 7(c), the O 1*s* spectra obtained at the HT-HACs/Ti-substrate interface are fit with four peaks: the above-mentioned PO, POH peaks of HA, the Ti-O peak at 529.6 eV and the Ti-OH peak at 532.5 eV. The Ti-O peak can be attributed to the surface oxide ion of Ti-substrate, and the peak at ΔBE about 3.0 eV from Ti-O peak can be assigned to the chemisorbed OH^- groups of Ti-OH [Healy & Ducheyne, 1992; Takadama et al., 2001]. Since the rapid solidification of molten

HA droplets during plasma spraying induces the formation of ACP within the as-sprayed HACs, XPS analysis results demonstrate that the hydrothermal treatment helps to promote the HA crystallization through the replenishment and the chemisorption of OH^- groups. The presence of Ti-OH bonding can enhance the bioactive properties of the HA coating by promoting the osteointegration process [Massaro et al., 2001].

5. Effect of the strengthening bond coats on the adhesive bonding strength of composite HA coatings

The most commonly used method of determining tensile bonding strength for the plasma-sprayed coatings is the criterion ASTM C633-01. The roughness of substrates is an important factor in achieving high bonding strength of plasma-sprayed HACs because the bonding of the HACs to metallic substrates appears to be mechanical interlocking in nature. There is less degree of chemical bonding in as-sprayed HACs. Ti-6Al-4V cylindrical rods with dimensions of 25.4 mm (ϕ) and 50 mm (l) are used as substrates for the tests. Each test specimen is an assembly composed of a substrate fixture, to which the HACs of 120 ± 10 μm are applied, and a loading fixture. The loading fixtures are also grit-blasted and attached to the surface of the HACs top coat using adhesive glue with an adhesive strength of about 60 MPa. After curing, the assemblies are subjected to tensile tests at a crosshead speed of 1 mm/min until failure. For the statistical significance of the following Weibull analysis, 20 specimens are tested for bonding strength measurements. Fig. 8 shows that the bonding strength of plasma-sprayed HACs is improved (ANOVA statistical analysis, $p < 0.05$) with applying the reinforced bond coats and post-heat treatments. The highest bonding strength about 39.9 ± 2.4 MPa is acquired for the HA/YSZ composite coating, and the HT-HACs shows a fairly high bonding strength of 38.9 ± 1.0 MPa. It can be recognized that the adhesive bonding strength is significant improved with applying the hydrothermal treatment and adding the YSZ bond coat compared to the other conditions.

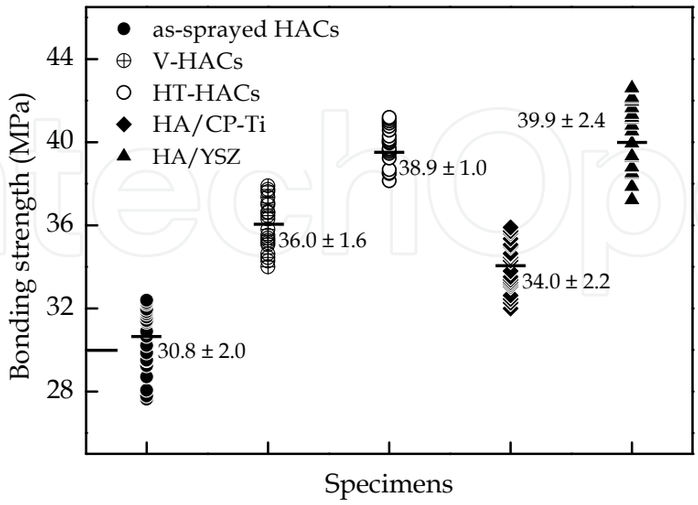

Fig. 8. Results of measuring bonding strength with the average value ± S.D. and the data fluctuation of as-sprayed HACs, V-HACs, HT-HACs, HA/CP-Ti and HA/YSZ composite coatings (S.D. means the standard deviation).

Referring to the cross-sectional features shown in Fig 5(b), the 600°C vacuum heat-treated specimen shows many vertical and apparent large cracks, which are resulted from crystallization-induced contraction of coating by the thermal dilatometry measurements [C.W. Yang& Lui, 2007]. Figure 4(c) represents cracks are obviously healed with the crystalline HA grains within the HT-HACs, which display a dense microstructure as shown in Fig. 5(c). It can be seen that the microstructural homogeneity with a self-healing effect occurred from the hydrothermal crystallization throughout the whole HA coating layers under the abundant saturated steam pressure environment. Although the bonding strength is improved with the crystallization of coating layers during vacuum heat treatments, however, it can be recognized that a detrimental effect of contraction-induced cracks accompanied with HA crystallization may result in the deterioration of bonding strength.

The representative failure surfaces of these coatings are shown in Fig. 9. According to ASTM C633-01, the variation of bonding strength in situ is suggested to be governed by the cohesive strength of coatings and the adhesive strength of a coating to a metal substrate. The affecting factors of the adhesive strength of a coating and substrate interface include the surface roughness of substrate and the residual stress. As for the cohesive strength of coating, the factors include the crystallinity and the densification of a coating, which appearing on the Young's modulus of a coating. A large area fraction of cohesive failure (co) can be commonly observed for high strength coatings [Kweh et al., 2000; C.W. Yang & Lui, 2008]. The cohesive failure is dominated by the microstructural features such as crystallinity, defects and lamellar texture. Compared with the failures of as-sprayed HACs shown in Fig. 9(a), the failure morphologies of HT-HACs (Fig. 9(b)) represent homogeneity and display a larger area fraction of cohesive failure, since strengthened coatings resulted from the self-healing effect of hydrothermal crystallization. In contrast, the decreased area fraction of adhesive failure (ad) indicates that the adhesion of HT-HACs to Ti-6Al-4V substrate is improved. Referring to the evidence from the XPS analysis as shown in Fig. 7(c), the hydrothermal treatment helps to promote the interfacial crystallization through the replenished and the chemisorbed OH^- groups, which results in a significant chemical bonding of HA coating to Ti-substrate interface.

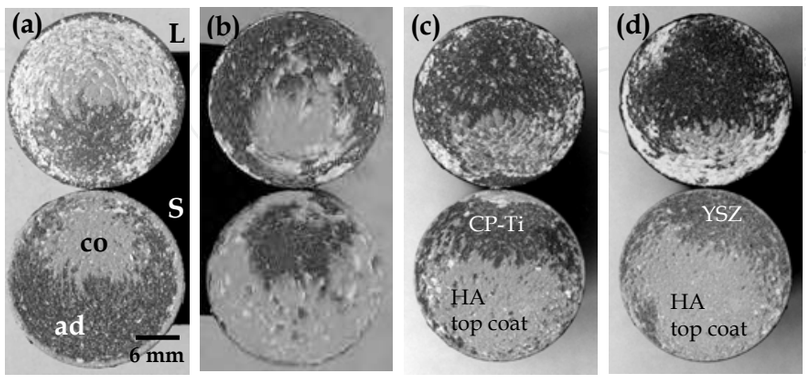

Fig. 9. Failure surfaces of (a) as-sprayed HAC, (b) HT-HACs, (c) HA/CP-Ti and (d) HA/YSZ composite coatings. The bonding strength measured is a manifestation of cohesive (co) and adhesive (ad) strength (L: loading fixture, S: substrate fixture).

Considering the HA/CP-Ti and HA/YSZ composite coatings, the decreased area fraction of adhesive failure (Fig. 9(c) and 9(d)) represents that the adhesion of HA top coat to substrate is also enhanced by adding YSZ and CP-Ti bond coats. The significant improvement of bonding strength for HA/CP-Ti and HA/YSZ composite coatings can be recognized that a higher surface roughness of CP-Ti and YSZ layers than grit-blasted Ti-6Al-4V substrate (Table 2) to provide better interfacial mechanical interlocking. The idea to further increase interlocking is to establish a chemical bonding between HA coating and bond coat. The evident shift of XPS binding energy of Ca 2*p* peak for the HA/YSZ interface compared with the as-sprayed HACs (Fig. 10) indicated that there is a significant interfacial diffusion [Vincent, 2000] for Ca ions at the interface of the HA top coat to the YSZ bond coat. However, there is no interfacial chemical reaction between the HA coating and the CP-Ti bond coat. Therefore, it can be related to the fact that the diffusion of Ca ions from HA matrix into the YSZ bond coat and the formation of chemical bonding of Ca-ZrO_2 [Khor et al., 2000; Chou & Chang, 2002b]. The interfacial chemical bonding can help to improve the bonding of HA/YSZ composite coatings.

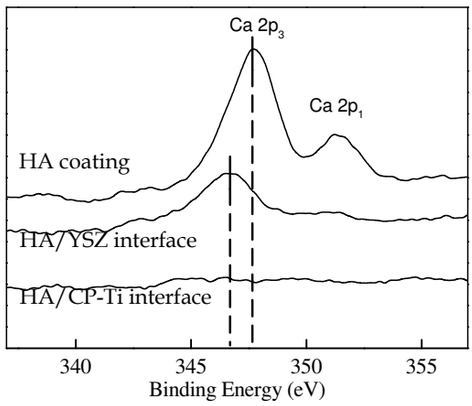

Fig. 10. XPS Ca 2*p* spectra for inter-diffusion analysis resulted from the as-sprayed HACs, the HA/YSZ bond coat interface and the HA/CP-Ti bond coat interface.

6. Evaluation of failure behaviors with statistical techniques

To characterize the strength data fluctuation, reliability, failure probability and failure mechanism of materials, a powerful statistical distribution function, which is called as the Weibull distribution function, was invented by Waloddi Weibull in 1937 and delivered his hallmark American paper in 1951 [Weibull, 1951]. He claimed that this model can be applied to a wide range of problems, and the Weibull models have been used in many different applications for solving a variety of problems from many different disciplines. Equation (3) shows the general form of the Weibull distribution function.

$$F(\sigma_i) = \int_{\sigma=0}^{\sigma=\sigma_i} f(\sigma)\, d\sigma = 1 - \exp\left[-\left(\frac{\sigma_i - \sigma_o}{\eta} \right)^m \right] \tag{3}$$

In Eq. (3), σ represents the bonding strength, and at least twenty specimens (n=20) are tested for the purpose of statistical significance of the analysis. $F(\sigma_i)$ is the cumulative failure probability corresponding to a bonding strength σ_i (i is the ranking of specimens). The

parameter m represents the Weibull modulus, η is the characteristic strength and σ_o is the minimum strength. The failure behavior of materials is determined by m, η and σ_o. The Weibull modulus, which controls the shape of function curves, is a measure of the variability of the data. The characteristic strength η corresponds to the strength at which the cumulative failure is 63.2%. The minimum strength σ_o means that the failure probability of HACs at applied stress below this value is zero. Fitting the bonding strength data into Eq. (3), the failure probability density function $f(\sigma)$ curves of the as-sprayed HACs, HA/CP-Ti and HA/YSZ composite coatings are plotted in Fig. 11(a). The cumulative failure probability $F(\sigma_i)$ is estimated using the Benard's median rank of Eq. (4), which is a very close approximated solution of a statistical function [Faucher & Tyson, 1988]. The reliability function $R(\sigma_i)$ with a relation of $R(\sigma_i) = 1–F(\sigma_i)$ is defined as the survival probability. Fig. 11(b) shows the natural logarithmic (ln) graphs for the cumulative failure probability at each corresponding bonding strength σ_i (i=1-20) of the specimens, it can graphically evaluate the Weibull modulus (m) from the slope of a least-squares fitting method of Eq. (5) at a maximum coefficient of determination (R^2).

$$F(\sigma_i) = \frac{i - 0.3}{n + 0.4} \tag{4}$$

$$\ln\ln\left(\frac{1}{1 - F(\sigma_i)}\right) = m\ln(\sigma_i - \sigma_o) - m\ln\eta \tag{5}$$

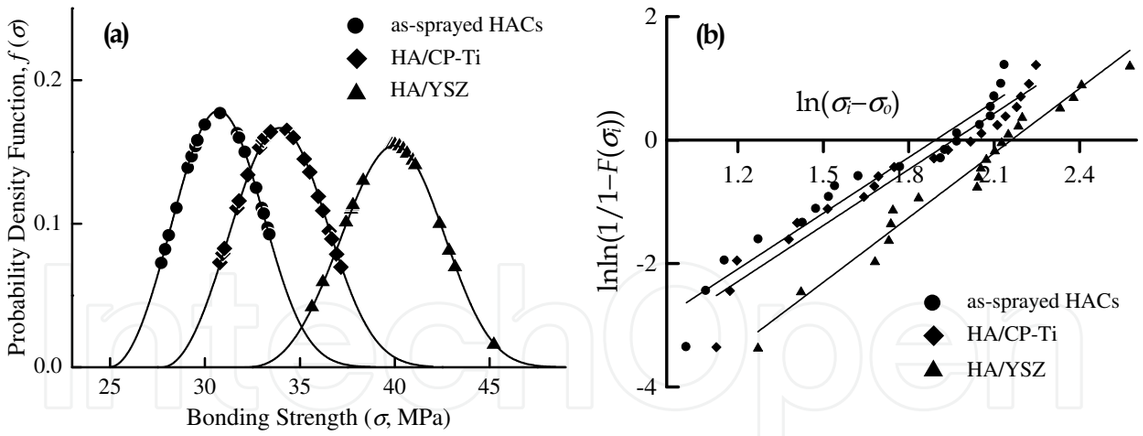

Fig. 11. (a) The failure probability density function $f(\sigma)$ curves, and (b) the Weibull distribution plots of the plasma-sprayed HACs, HA/CP-Ti and HA/YSZ composite coatings.

Since the Weibull distribution function is used to model the reliability and the failure behavior of materials, a failure rate function $\lambda(\sigma_i)$ shown in Eq. (6) at each corresponding bonding strength is defined for evaluating the failure behaviors [Burrow et al., 2004].

$$\lambda(\sigma_i) = \frac{f(\sigma_i)}{R(\sigma_i)} = \frac{m}{\eta^m}(\sigma_i - \sigma_o)^{m-1} \tag{6}$$

The examination of the Weibull modulus listed in Table 4 represents that HACs are reliable materials with a wear-out failure model (m > 1) of increasing failure rate (IFR). Figure 12 shows the failure rate function ($\lambda(\sigma)$) and reliability function ($R(\sigma)$) curves of the as-sprayed HAC, HA/CP-Ti and HA/YSZ composite coatings. These curves start from the minimum strength (σ_o), which implies the failure probability of HACs less than this strength is zero and the reliability of HACs is 1.0. The minimum strength can be recognized as the safe loading level for the plasma-sprayed HACs. Meanwhile, knowledge of the Weibull distribution function can provide further explanation for the strengthening effect of reinforced YSZ and CP-Ti bond coats on the bonding strength of as-sprayed HACs, and it can be used to determine which coating has higher uniformity and reliability. The Weibull modulus is also a measure of the variability of the data, which being larger as the degree of bonding strength fluctuation decreases. It is evident that the failure probability density function (Fig. 11(a)) and the failure rate (Fig. 12(a)) curves shift to the higher bonding strength and produce a concentrated data distribution for the HA/YSZ composite coating. The YSZ bond coat effectively enhances the bonding strength of plasma-sprayed HAC, and helps to acquire more stable HACs with less reliability decrease (Fig. 12(b)) while the loading exceeds the minimum strength.

Samples	Weibull Modulus, m	Minimum strength, σ_o (MPa)	Characteristic strength, η (MPa)
As-sprayed HACs	3.0	24.9	31.8
HA/CP-Ti	3.0	27.7	35.0
HA/YSZ	3.5	32.1	40.9

Table 4. Results of Weibull model analysis for the HACs

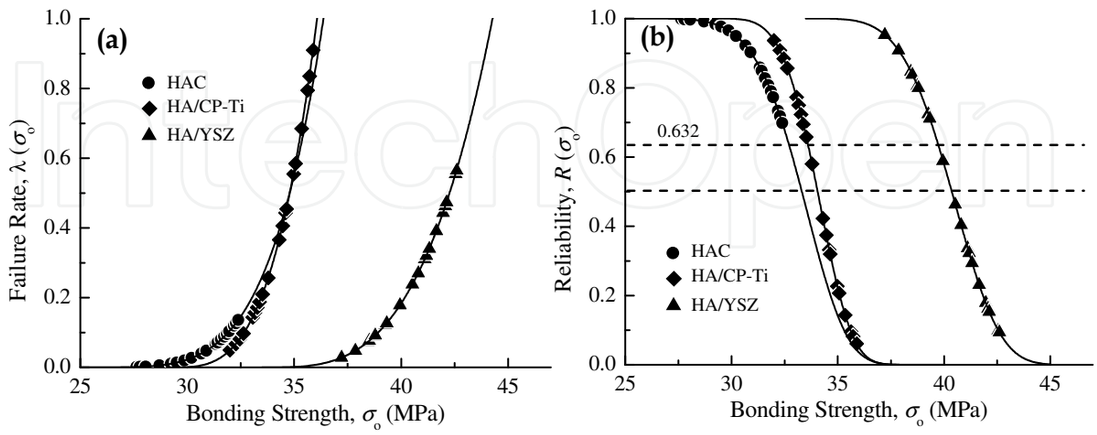

Fig. 12. (a) The failure rate function $\lambda(\sigma)$ curves, and (b) the reliability function $R(\sigma)$ curves.

7. Conclusion

The evolution of microstructural features, biological responses, crystallization kinetics, tensile mechanical properties and failure behaviors of post-spray heat-treated HACs by the vacuum heating and the hydrothermal treatment are evaluated. Applying heat treatments is an effective way to improve the crystallization state, biological responses and adhesive bonding strength of plasma-sprayed HACs. Compared with these two heat treatments, the hydrothermal treatment is more favorable to eliminate the impurity phases and ACP than high temperature heat treatments in vacuum. Hydrothermal crystallization, which proceeded within a saturated steam environment, significantly improves the microstructural homogeneity, coating density and HA/Ti-substrate interfacial reaction of plasma-sprayed HACs through the self-healing effect with the grain growth of the crystalline HA. In addition, hydrothermally-treated HACs display a higher new bone healing and apposition index than the as-sprayed and vacuum heat-treated HACs. The crystallization of plasma-sprayed HACs during heat treatments is second-order Arrhenius reaction kinetics. The effect of ambient heating atmosphere with a saturated steam pressure is an important factor for the hydrothermal treatment to further promote HA crystallization rate at lower heating temperatures. The addition of CP-Ti and YSZ as intermediate strengthening bond coats between HA/Ti-substrate can significantly enhance the adhesive bonding strength of plasma-sprayed HACs. In addition to the higher mechanical interlocking between HA top coat and bond coat interface, a chemical bonding resulted from the interfacial diffusion at the HA/YSZ bond coat interface can further improve the adhesive bonding strength for the HA/YSZ composite coating. Fractures with less area percentage of interfacial failure are indicative of a better adhesion of a coating. According to the results of Weibull model analysis, plasma-sprayed HACs represent a wear-out failure behavior (the Weibull modulus, $m > 1$) with increasing failure rate. The adhesion and survival probability of plasma-sprayed HACs are improved by adding the YSZ bond coat to form a HA/YSZ composite coating.

8. Acknowledgment

This study was financially supported by the National Science and Council of Taiwan (Contract No. NSC 100-2221-E-150-037) for which we are grateful.

9. References

Akahori, T.; Niinomi, M.; Fukui, H. & Suzuki, A. (2004). Fatigue, Fretting Fatigue and Corrosion Characteristics of Biocompatible Beta Type Titanium Alloy Conducted with Various Thermo-mechanical Treatments. *Materials Transactions*, Vol.45, No.5, pp. 1540-1548, ISSN 1345-9678.

Bauer, T.W.; Geesink, R.C.T.; Zimmerman, R. & McMahon, J.T. (1991). Hydroxyapatite-coated Femoral Stems: Histological Analysis of Components Retrieved at Autopsy. *The Journal of Bone and Joint Surgery [Am]*, Vol.73A, pp. 1439-1452, ISSN 1535-1386.

Ben-Nissan, B. & Choi, A.H. (2006). Sol-gel Production of Bioactive Nano-coatings for Medical Applications Part 1: An Introduction. *Nanomedicine*, Vol.1, pp. 311-319, ISSN 1549-9634.

Bourdin, E.; Fauchais, P. & Boulos, M. (1983). Transient Heat Conduction under Plasma Conditions. *International Journal of Heat and Mass Transfer*, Vol.26, pp. 567-582, ISSN 0017-9310.

Bucholz, R.W.; Carlton, A. & Holmes, R.E. (1989). Interporous Hydroxyapatite as a Bone Graft Substitute in Tibial Plateau Fractures. *Clinical Orthopaedics and Related Research*, Vol.240, pp. 53-62, ISSN 0009-921X.

Burrow, M.F.; Thomas, D.; Swain, M.V. & Tyas, M.J. (2004). Analysis of Tensile Strengths Using Weibull Statistics. *Biomaterials*, Vol.25, pp. 5031-5035, ISSN 0142-9612.

Callaghan, J.J. (1993) Current Concepts Review: The Clinical Results and Basic Science of Total Hip Arthroplasty with Porous-coated Prostheses. *The Journal of Bone and Joint Surgery [Am]*, Vol.75A, pp. 299-310, ISSN 1535-1386.

Campos, A.L.; Silva, N.T.; Melo, F.C.L.; Oliverira, M.A.S. & Thim, G.P. (2002). Crystallization Kinetics of Orthorhombic Mullite from Diphasic. *Journal of Non-Crystalline Soilds*, Vol.304, pp. 19-24, ISSN 0022-3093.

Cannillo, V., Lusvarghi, L, & Sola, A. (2008). Production and Characterization of Plasma-sprayed TiO_2-Hydroxyapatite Functionally Graded Coatings. *Journal of the European Ceramic Society*, Vol.28, pp. 2161-2169, ISSN 0955-2219.

Cao, Y.; Weng, J.; Chen, J.; Feng, J.; Yang, Z. & Zhang, X. (1996). Water Vapor-treated Hydroxyapatite Coatings after Plasma Spraying and Their Characteristics. *Biomaterials*, Vol.17, pp. 419-424, ISSN 0142-9612.

Chang, E.; Chang, W.J.; Wang, B.C. & Yang, C.Y. (1997). Plasma Spraying of Zirconia-reinforced Hydroxyapatite Composite Coatings on Titanium: Part I. Phase, Microstructure and Bonding Strength. *Journal of Materials Science: Materials in Medicine*, Vol.8, pp. 193-200, ISSN 0957-4530.

Chang, C.; Huang, J.; Xia, J. & Ding, C. (1999). Study on Crystallization Kinetics of Plasma Sprayed Hydroxyapatite Coating. *Ceramics International*, Vol.25, pp. 479-483, ISSN 0272-8842.

Chen, J.; Tong, W.; Cao, Y.; Feng, J. & Zhang, X. (1997). Effect of Atmosphere on Phase Transformation in Plasma-sprayed Hydroxyapatite Coatings during Heat Treatment. *Journal of Biomedical Materials Research*, Vol.34, pp. 15-20, ISSN 0021-9304.

Choi, J.W.; Kong, Y.M. & Kim, H.E. (1998). Reinforcement of Hydroxyapatite Bioceramic by Addition of Ni_3Al and Al_2O_3. *Journal of the American Ceramic Society*, Vol.81, pp. 1743-1748, ISSN 0002-7820.

Chou, B.Y. & Chang, E. (2002a). Phase Transformation during Plasma Spraying of Hydroxyapatite-10-wt%-Zirconia Composite Coating. *Journal of the American Ceramic Society*, Vol.85, pp. 661-669, ISSN 0002-7820.

Chou, B.Y. & Chang, E. (2002b). Plasma-sprayed Zirconia Bond Coat as an Intermediate Layer for ydroxyapatite Coating on Titanium Alloy Substrate. *Journal of Materials Science: Materials in Medicine*, Vol.13, pp. 589-595, ISSN 0957-4530.

Cook, S.D.; Thomas, K.; Kay, J.F. & Jarcho, M. (1988). Hydroxylapatite Coated Titanium for Orthopaedic Implant Applications. *Clinical Orthopaedics and Related Research*, Vol.232, pp. 225-243, ISSN 0009-921X.

Cook, S.D.; Thomas, K.A.; Delton, J.E.; Volkman, T.K.; Whitecloud, T.S. & Key, J.F. (1992). Hydroxyapatite Coating of Porous Implants Improves Bone Ingrowth and Interface Attachment Strength. *Journal of Biomedical Materials Research*, Vol.26, pp. 989-101, ISSN 0021-9304.

de Groot, K.; Klein, C.P.A.T.; Wolke, J.G.C. & de Bliek-Hogervost, J.M.A. (1990). Chemistry of Calcium Phosphate Bioceramics, In: *CRC Handbook of Bioactive Ceramics. Vol. II*, T. Yamamuro, L.L. Hench & J. Wilson, (Eds.), 3-16. CRC Press Inc., ISBN 978-084-9332-42-5, Boca Raton: Taylor & Francis.

Ducheyne, P.; Radin, S. & King, L. (1993). The Effect of Calcium Phosphate Ceramic Composition and Structure on *In Vitro* Behavior: I. Dissolution. *Journal of Biomedical Materials Research*, Vol.27, pp. 25-34, ISSN 0021-9304.

Engh, C.A.; Bobyn, J.D. & Glassman, A.H. (1987). Porous-coated Hip Replacement. *The Journal of Bone and Joint Surgery [Br]*, Vol.69B, pp. 45-55, ISSN 0301-620X.

Faucher, B. & Tyson, W.R. (1988). On the Determination of Weibull Parameters. *Journal of Materials Science Letters*, Vol.7, pp. 1199-1203, ISSN 0261-8028.

Fauchias, P.; Coudert, J.F.; Vardelle, M.; Vardelle, A. & Denoirjean, A. (1992). Diagnostics of Thermal Spray Plasma Jets. *Journal of Thermal Spray Technology*, Vol.1, pp. 117-128, ISSN 1059-9630.

Feng, C.F.; Khor, K.A.; Liu, E.J. & Cheang, P. (2000). Phase Transformations in Plasma Sprayed Hydroxyapatite Coatings. *Scripta Materialia*, Vol.42, pp. 103-109, ISSN 1359-6462.

Fu, L.; Khor, K.A. & Lim, J.P. (2001). The Evaluation of Powder Processing on Microstructure and Mechanical Properties of Hydroxyapatite (HA) /Yttria Stabilized Zirconia (YSZ) Composite Coatings. *Surface and Coatings Technology*, Vol.140, pp. 263-268, ISSN 0257-8972.

Geesink, R.G.T.; de Groot, K. & Klein, C.P.A.T. (1987). Chemical Implant Fixation Using Hydroxyapatite Coatings. *Clinical Orthopaedics and Related Research*, Vol.225, pp. 147-170, ISSN 0009-921X.

Geesink, R.G.T.; de Groot, K. & Klein, C.P.A.T. (1988). Bonding of Bone to Apatite-coated Implants. *The Journal of Bone and Joint Surgery [Br]*, Vol.70B, pp. 17-22, ISSN 0301-620X.

Gross, K.A. & Berndt, C.C. (1998). Thermal Processing of Hydroxyapatite for Coating Production. *Journal of Biomedical Materials Research*, Vol.39, pp. 580-587, ISSN 0021-9304.

Gross, K.A.; Gross, V. & Berndt, C.C. (1998). Thermal Analysis of Amorphous Phases in Hydroxyapatite Coatings. *Journal of the American Ceramic Society*, Vol.81, pp. 106-112, ISSN 0002-7820.

Healy, K.E. & Ducheyne, P. (1992). The Mechanisms of Passive Dissolution of Titanium in a Model Physiological Environment. *Journal of Biomedical Materials Research*, Vol.26, pp. 319-338, ISSN 0021-9304.

Hench, L.L. (1991). Bioceramics: From Concept to Clinic. *Journal of the American Ceramic Society*, Vol.74, No.7, pp. 1487-1510, ISSN 0002-7820.

Holmes, R.E.; Bucholz, R.W. & Mooney, V. (1986). Porous Hydroxyapatite as a Bone-graft Substitute in Metaphyseal Defects. *The Journal of Bone and Joint Surgery [Am]*, Vol.68A, pp. 904-911, ISSN 1535-1386.

Huang, L.Y.; Xu, K.W. & Lu, J. (2000). A Study of the Process and Kinetics of Electrochemical Deposition and the Hydrothermal Synthesis of Hydroxyapatite Coatings. *Journal of Materials Science: Materials in Medicine*, Vol.11, pp. 667-673, ISSN 0957-4530.

Ingham, H.S. & Shepard, A.P. (1965). *Plasma Flame Process*, METCO Inc., p. 11, Westburg, Long Island, New York, USA.

Jansen, J.A.; van de Waerden, J.P.C.M.; Wolke, J.G.C. & de Groot, K. (1991). Histologic Evaluation of the Osseous Adaptation to Titanium and Hydroxy-apatite-coated Titanium Implants. *Journal of Biomedical Materials Research*, Vol.25, pp. 973-989, ISSN 0021-9304.

Jarcho, M. (1981). Calcium Phosphate Ceramics as Hard Tissue Prosthetics. *Clinical Orthopaedics and Related Research*, Vol.157, pp. 259-278, ISSN 0009-921X.

Ji H. & Marquis, P.M. (1993). Effect of Heat Treatment on the Microstructure of Plasma-sprayed Hydroxyapatite Coating. *Biomaterials*, Vol.14, pp. 64-68, ISSN 0142-9612.

Khor, K.A.; Fu, L.; Lim, J.P. & Cheang, P. The Effects of ZrO2 on the Phase Compositions of Plasma Sprayed HA/YSZ Composite Coatings. (2000). *Materials Science and Engineering A*, Vol.276, pp. 160-166, ISSN 0921-5093.

Kokubo, T.; Hayashi, T.; Sakka, S.; Kitsugi, T. & Yamamuro, T. (1987). Bonding between Bioactive Glasses, Glass-ceramics or Ceramics in a Simulated Body Fluid. *Journal of the Ceramic Society of Japan*, Vol.95, pp. 785-791, ISSN 0372-7718.

Kuroda, D.; Niinomi, M.; Morinaga, M.; Kato, Y. & Yashiro, T. (1998). Design and Mechanical Properties of New Beta Type Titanium Alloys for Implant Materials. *Materials Science and Engineering A*, Vol.243, pp. 244-249, ISSN 0921-5093.

Kurzweg, H.; Heimann, R.B. & Troczynski, T. (1998). Adhesion of Thermally Sprayed Hydroxyapatite Bond-coat Systems Measured by a Novel Peel Test. *Journal of Materials Science: Materials in Medicine*, Vol.9, pp. 9-16, ISSN 0957-4530..

Kweh, S.W.K.; Khor, K.A.; & Cheang, P. (2000). Plasma-sprayed Hydroxyapatite (HA) Coatings with Flame-spheroidized Feedstock: Microstructure and Mechanical Properties. *Biomaterials*, Vol.21, pp. 1223-1234, ISSN 0142-9612.

Lamy, D.; Pierre, A.C. & Heimann, R.B. (1996). Hydroxyapatite Coatings with a Bond Coat of Biomedical Implants by Plasma Projection. *Journal of Materials Research*, Vol.11, pp. 680-686, ISSN 0884-2914.

Lee, Y.P.; Wang, C.K.; Huang, T.H.; Chen, C.C.; Kao, C.T. & Ding, S.J. (2005). *In vitro* Characterization of Post Heat-treated Plasma-sprayed Hydroxyapatite Coatings. *Surface and Coatings Technology*, Vol.197, pp. 367-374, ISSN 0257-8972.

Lintner, F.; Böhm, G.; Huber, M. & Scholz, R. (1994). Histology of Tissue Adjacent to an HAC-coated Femoral Prostheses: A Case Report. *The Journal of Bone and Joint Surgery [Br]*, Vol.76B, pp. 824-830, ISSN 0301-620X.

Liu, C.; Huang, Y.; Shen, W. & Cui, J. (2001). Kinetics of Hydroxyapatite Precipitation at pH 10 to 11. *Biomaterials*, Vol.22, pp. 301-306, ISSN 0142-9612.

Liu, X.; Chu, P.K. & Ding, C. (2007). Formation of Apatite on Hydrogenated Amorphous Silicon (a-Si:H) Film Deposited by Plasma-enhanced Chemical Vapor Deposition. *Materials Chemistry and Physics*, Vol.101, pp. 124-128, ISSN 0254-0584.

Lu, Y.P.; Song, Y.Z.; Zhu, R.F.; Li, M.S. & Lei, T.Q. (2003). Factors Influencing Phase Compositions and Structure of Plasma Sprayed Hydroxyapatite Coatings during Heat Treatment. *Applied Surface Science*, Vol.206, pp. 345-354, ISSN 0169-4332.

Lu, Y.P.; Li, M.S.; Li, S.T.; Wang, Z.G. & Zhu, R.F. (2004). Plasma-sprayed Hydroxyapatite + Titanium Composite Bond Coat for Hydroxyapatite Coating on Titanium Substrate. *Biomaterials*, Vol.25, pp. 4393-4403, ISSN 0142-9612.

Lugscheider, L.; Remer, P. & Nyland, A. (1996). High Velocity Oxy Fuel Spraying: An Alternative to the Established APS-process for Production of Bioactive Coatings, In:

Proceedings of the Tenth International Conference on Surface Modification Technologies, Singapore, T.S. Sudarsan, K.A. Khor, & M. Jeandin, (Eds.), 717-727.

Massaro, C.; Baker, M.A.; Cosentino, F.; Ramires, P.A.; Klose, S. & Milella, E. (2001). Surface and Biological Evaluation of Hydroxyapatite-based Coatings on Titanium Deposited by Different Techniques. *Journal of Biomedical Materials Research*, Vol.58B, pp. 651-657, ISSN 0021-9304.

Munting, E.; Verhelpen, M.; Li, F. & Vincent, A. (1990). Contribution of Hydroxy-apatite Coatings to Implant Fixation, In: *CRC Handbook of Bioactive Ceramics, Vol. II*, T. Yamamuro, L.L. Hench & J. Wilson, (Eds.), 143-148, CRC Press Inc., ISBN 978-084-9332-42-5, Boca Raton: Taylor & Francis.

Niinomi, M.; Kuroda, D.; Fukunaga, K.; Morinaga, M.; Kato, Y.; Yashiro, T. & Suzuki, A. (1999). Corrosion Wear Fracture of New β Type Biomedical Titanium Alloys, *Materials Science and Engineering A*, Vol.263, pp. 193-199, ISSN 0921-5093.

Niinomi, M. (2001). Recent Metallic Materials for Biomedical Applications. *Metallurgical and Materials Transactions A*, Vol.32A, pp. 477-486, ISSN 1073-5623.

Niinomi, M.; Hattori, T.; Morikawa, K.; Kasuga, T.; Suzuki, A.; Fukui, H. & Niwa, S. (2002). Development of Low Rigidity β-type Titanium Alloy for Biomedical Applications. *Materials Transactions*, Vol.43, No.12, pp. 2970-2977, ISSN 1345-9678.

Ozeki, K.; Aoki, H. & Fukui, Y. (2006). Dissolution Behavior and In Vitro Evaluation of Sputtered Hydroxyapatite Films Subject to a Low Temperature Hydrothermal Treatment. *Journal of Biomedical Materials Research*, Vol.76A, pp. 605-613, ISSN 0021-9304.

Peng, P.; Kumar, S.; Voelcker, N.H.; Szili, E.; Smart, R.S.C. & Griesser, H.J. (2006). Thin Calcium Phosphate Coatings on Titanium by Electrochemical Deposition in Modified Simulated Body Fluid. *Journal of Biomedical Materials Research*, Vol.76A, pp. 347-355, ISSN 0021-9304.

Pfender, E. (1994). Plasma Jet behavior and Modeling Associated with the Plasma Spray Process. *Thin Solid Films*, Vol.238, pp. 228-241, ISSN 0040-6090.

Pilliar, P.M.; Cameron, H.U.; Binnington, A.G. & Szivek, J.A. (1979). Bone Ingrowth and Stress Shielding with a Porous Surface Coated Fracture Fixation Plate. *Journal of Biomedical Materials Research*, Vol.13, pp. 799-810, ISSN 0021-9304.

Radin, S.R. & Ducheyne, P. (1993). Effect of Calcium Phosphate Ceramic Composition and Structure on *in vitro* Behavior. II. Precipitation. *Journal of Biomedical Materials Research*, Vol.27, pp. 35-45, ISSN 0021-9304.

Roeder, R.K.; Converse, G.L.; Leng, H. & Yue, W. (2006). Kinetics Effects on Hydroxyapatite Whiskers Synthesized by the Chelate Decomposition Method. *Journal of the American Ceramic Society*, Vol.89, Mo.7, pp. 2096-2104, ISSN 0002-7820.

Sato, M.; Aslani, A.; Sambito, M.A.; Kalkhoran, N.M.; Slamovich, E.B. & Webster, T.J. (2008). Nanocrystalline Hydroxyapatite/Titania Coatings on Titanium Improves Osteoblast Adhesion. *Journal of Biomedical Materials Research*, Vol.84A, pp. 265-272, ISSN 0021-9304.

Schreurs, B.W.; Huiskes, R.; Buma, P. & Slooff, T.J.J.H. (1996). Biomechanical and Histological Evaluation of a Hydroxyapatite-coated Titanium Femoral Stem Fixed with an Intramedullary Morsellized Bone Grafting Technique: An Animal Experiment on Goats. *Biomaterials*, Vol.17, pp. 1177-1186, ISSN 0142-9612.

Standard Test Method for Adhesion and Cohesion Strength of Thermal Spray Coatings. ASTM C633-01, West Conshohocken, PA, USA.

Sturgeon, A.J. & Harvey, M.D.F. (1995). High Velocity Oxyfuel Spraying of Hydroxyapatite. *Proceedings of ITSC'95*, pp. 933-938, Kobe, Japan, May, 1995.

Sunderman, F.W.Jr.; Hopfer, S.M.; Swift, T.; Rezuke, W.N.; Ziebka, L.; Highman, P.; Edwards, B.; Folcik, M. & Gossling, H.R. (1989). Cobalt, Chromium, and Nickel Concentrations in Body Fluids of Patients with Porous-coated Knee or Hip Prostheses. *Journal of Orthopaedic Research*, Vol.7, pp. 307-315, ISSN 1554-527X.

Suryanarayanan, R. (1993). *Plasma Spraying: Theory and Applications*, World Scientific Publishing Co. Pte. Ltd., p. 4, ISBN 978-981-02-1363-3.

Takadama, H.; Kim, H.M.; Kokubo, T. & Nakamura, T. (2001). An X-ray Photoelectron Spectroscopy Study of the Process of Apatite Formation on Bioactive Titanium Metal. *Journal of Biomedical Materials Research*, Vol.55, pp. 185-193, ISSN 0021-9304.

Tong, W.; Chen, J.; Cao, Y.; Lu, L.; Feng, J. & Zhang, X. (1997). Effect of Water Vapor Pressure and Temperature on the Amorphous-to-Crystalline HA Conversion during Heat Treatment of HA Coatings. *Journal of Biomedical Materials Research*, Vo.36, pp. 242-245, ISSN 0021-9304.

van Audekercke, R. & Martens, M. (1984). Mechanical Properties of Cancellous Bone, In: *Natural and Living Biomaterials*, G.W. Hastings & P. Ducheyne, (Eds.), 89-98, CRC Press Inc., ISBN 978-084-9362-64-4, Boca Raton: Taylor & Francis.

Vincent, C.B. (2000). *Handbook of Monochromatic XPS Spectra, The Elements of Native Oxides*, John Wiley and Sons, Ltd., 49-53, ISBN 978-047-1492-65-8, England.

Wang, B.C.; Chang, E.; Yang, C.Y.; & Tu, D. (1993a). A Histomorphometric Study on Osteoconduction and Osseointegration of Titanium Alloy with and without Plasma-sprayed Hydroxyapatite Coating Using Back-scattered Electron Images. *Journal of Materials Science: Materials in Medicine*, Vol.4, pp. 394-403, ISSN 0957-4530.

Wang, B.C.; Chang, E.; Yang, C.Y.; Tu, D. & Tsai, H. (1993b). Characteristics and Osteoconductivity of Three Different Plasma-sprayed Hydroxyapatite Coatings. *Surface and Coatings Technology*, Vol.58, pp. 107-117, ISSN 0257-8972.

Wang, B.C.; Chang, E.; Lee, T.M. & Yang, C.Y. (1995). Changes in Phases and Crystallinity of Plasma-sprayed Hydroxyapatite Coatings under Heat Treatment: A Quantitative Study. *Journal of Biomedical Materials Research*, Vol.29, pp. 1483-1492, ISSN 0021-9304.

Wei, M.; Ruys, A.J.; Milthorpe, B.K. & Sorrell, C.C. (2005). Precipitation of Hydroxyapatite Nano-particles: Effects of Precipitation Method on Electrophoretic Deposition. *Journal of Materials Science: Materials in Medicine*, Vol.16, pp. 319-324, ISSN 0957-4530.

Weibull, W. (1951). A Statistical Distribution Function of Wide Applicability. *Journal of Applied Mechanics*, Vol.18, pp. 293-297, ISSN 0021-8936.

Weng J.; Liu X.; Zhang X. & de Groot, K. (1996). Integrity and Thermal Decomposition of Apatite in Coatings Influenced by Underlying Titanium during Plasma Spraying and Post-heat-treatment. *Journal of Biomedical Materials Research*, Vol.30, pp. 5-11, ISSN 0021-9304.

Wolke, J.G.C.; Klein, C.P.A.T. & de Groot, K. (1992). Bioceramics for Maxillofacial Applications, In *Bioceramics and the Human Body*, A. Ravaglioli & A. Krajewski, (Eds.), 166-180. Elsevier Science Publishers Ltd., ISBN 978-185-1667-48-2, England.

Yang, C.W.; Lee, T.M.; Lui, T.S. & Chang, E. (2006). Effect of Post Vacuum Heating on the Microstructural Feature and Bonding Strength of Plasma-sprayed Hydroxyapatite Coatings. *Materials Science and Engineering C*, Vol.26, pp. 1395-1400, ISSN 0928-4931.

Yang, C.W. & Lui, T.S. (2007). Effect of Crystallization on the Bonding Strength and Failures of Plasma-sprayed Hydroxyapatite. *Materials Transactions*, Vol.48, No.2, pp. 211-218, ISSN 1345-9678.

Yang, C.W. & Lui, T.S. (2008). The Self-healing Effect of Hydrothermal Crystallization on the Mechanical and Failure Properties of Hydroxyapatite Coatings. *Journal of the European Ceramic Society*, Vol.28, pp. 2151-2159, ISSN 0955-2219.

Yang, C.W. & Lui, T.S. (2009). Kinetics of Hydrothermal Crystallization under Saturated Steam Pressure and the Self-healing Effect by Nanocrystallite for Hydroxyapatite Coatings. *Acta Biomaterialia*, Vol.5, pp. 2728-2737, ISSN 1742-7061.

Yang, C.Y.; Wang, B.C.; Chang, E. & Wu, B.C. (1995). Bond Degradation at the Plasma-sprayed HA Coating/Ti-6Al-4V Alloy Interface: An *in vitro* Study. *Journal of Materials Science: Materials in Medicine*, Vol.6, pp. 258-265, ISSN 0957-4530.

Yang, C.Y.; Lin, R.M.; Wang, B.C.; Lee, T.M.; Chang, E.; Hang, Y.S. & Chen, P.Q. (1997). *In Vitro* and *in Vivo* Mechanical Evaluations of Plasma-sprayed Hydroxyapatite Coatings on Titanium Implants: The Effect of Coating Characteristics. *Journal of Biomedical Materials Research*, Vol.37, pp. 335-345, ISSN 0021-9304.

Yang, C.Y.; Lee, T.M.; Yang, C.W.; Chen, L.R.; Wu, M.C. & Lui, T.S. (2007). The *in vitro* and *in vivo* Biological Responses of Plasma-sprayed Hydroxyapatite Coatings with Post-hydrothermal Treatment. *Journal of Biomedical Materials Research*, Vol.83A, pp. 263-271, ISSN 0021-9304.

Yang, C.Y.; Yang, C.W.; Chen, L.R.; Wu, M.C.; Lui, T.S; Kuo, A. & Lee, T.M. (2009). Effect of Vacuum Post-heat Treatment of Plasma-sprayed Hydroxyapatite Coatings on Their *in vitro* and *in vivo* Biological Responses. *Journal of Medical and Biological Engineering*, Vol.29, No.6, pp. 296-302, ISSN 1609-0985.

Yang, Y.; Kim, K.H.; Agrawal, C.M. & Ong, J.L. (2003). Influence of Post-deposition Heating Time and the Presence of Water Vapor on Sputter-coated Calcium Phosphate Crystallinity. *Journal of Dental Research*, Vol.82, pp. 833-837, ISSN 1544-0591.

Yang, Y. & Ong, J.L. (2003). Bond Strength, Compositional, and Structural Properties of Hydroxyapatite Coating on Ti, ZrO_2-coated Ti, and TPS-coated Ti Substrate. *Journal of Biomedical Materials Research*, Vol.64A, pp. 509-516, ISSN 0021-9304.

Yu, L.G.; Khor, K.A.; Li, H. & Cheang, P. (2003). Effect of Spark Plasma Sintering on the Microstructure and *in vitro* Behavior of Plasma Sprayed HA Coatings. *Biomaterials*, Vol.24, pp. 2695-2705, ISSN 0142-9612.

Yuan, H.; Yang, Z.; de Bruijn, J.D.; de Groot, K. & Zhang, X. (2001). Material-dependent Bone Induction by Calcium Phosphate Ceramics: A 2.5-year Study in Dog. *Biomaterials*, Vol.22, pp. 2617-2623, ISSN 0142-9612.

Zhang, H.; Li, S.; & Yan, Y. (2001). Dissolution Behavior of Hydroxyapatite Powder in Hydrothermal Solution. *Ceramics International*, Vol.27, pp. 451-454, ISSN 0272-8842.

Zheng, X.; Huang, M. & Ding, C. (2000). Bond Strength of Plasma-sprayed Hydroxyapatite/Ti Composite Coatings. *Biomaterials*, Vol.21, pp. 841-849, ISSN 0142-9612.

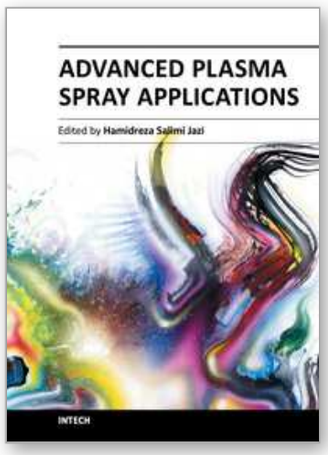

Advanced Plasma Spray Applications
Edited by Dr. Hamid Jazi

ISBN 978-953-51-0349-3
Hard cover, 250 pages
Publisher InTech
Published online 21, March, 2012
Published in print edition March, 2012

Recently, plasma spray has been received a large number of attentions for various type of applications due to the nature of the plasma plume and deposition structure. The plasma gas generated by the arc, consists of free electrons, ionized atoms, some neutral atoms, and undissociated diatomic molecules. The temperature of the core of the plasma jet may exceed up to 30,000 K. Gas velocity in the plasma spray torch can be varied from subsonic to supersonic using converging-diverging nozzles. Heat transfer in the plasma jet is primarily the result of the recombination of the ions and re-association of atoms in diatomic gases on the powder surfaces and absorption of radiation. Taking advantages of the plasma plume atmosphere, plasma spray can be used for surface modification and treatment, especially for activation of polymer surfaces. I addition, plasma spray can be used to deposit nanostructures as well as advanced coating structures for new applications in wear and corrosion resistance. Some state-of-the-art studies of advanced applications of plasma spraying such as nanostructure coatings, surface modifications, biomaterial deposition, and anti wear and corrosion coatings are presented in this book.

INTECH
open science | open minds

InTech Europe
University Campus STeP Ri
Slavka Krautzeka 83/A
51000 Rijeka, Croatia
Phone: +385 (51) 770 447
Fax: +385 (51) 686 166
www.intechopen.com

InTech China
Unit 405, Office Block, Hotel Equatorial Shanghai
No.65, Yan An Road (West), Shanghai, 200040, China
中国上海市延安西路65号上海国际贵都大饭店办公楼405单元
Phone: +86-21-62489820
Fax: +86-21-62489821

IntechOpen